JOURNAL OF SOLID STATE CHEMISTRY 120, 170–174 (1995)

Preparation, Crystal Structure, and Metal-to-Insulator Transition of $EuNiO_3$

J. A. Alonso,[1] M. J. Martínez-Lope, and I. Rasines

Instituto de Ciencia de Materiales de Madrid, C.S.I.C. Serrano 113, 28006 Madrid, Spain

Received April 20, 1995; in revised form July 28, 1995; accepted August 1, 1995

Polycrystalline $EuNiO_3$ has been prepared by a citrate technique and a subsequent thermal treatment at 1000°C under 200 bar of oxygen pressure. The crystal structure was refined by the Rietveld method from X-ray powder diffraction data. $EuNiO_3$ is an orthorhombic perovskite with $a = 5.2938(1)$, $b = 5.4560(1)$, $c = 7.5359(2)$ Å, space group *Pbnm*, $Z = 4$. A bond valence study shows that Eu and Ni cations are slightly over- and underbonded, respectively, giving rise to compressive/tensile stresses in the Eu–O/Ni–O bonds which are thought to be in the origin of the metastable character of the structure. The trend of Ni to increase its binding power leads to the observed distortion of the NiO_6 octahedra. The first-order metal-to-insulator (MI) transition was studied by differential scanning calorimetry ($T_{MI} = 463$ or 459 K on the heating or cooling runs, respectively). The corresponding heat flow is about half the value observed for $NdNiO_3$, in which a magnetic transition is associated to the MI transition.

INTRODUCTION

Recently the perovskites $RNiO_3$ (R = rare earth) have attracted considerable attention since they are among the few transition metal oxides that exhibit metallic properties or metal-to-insulator (MI) transitions (1). In this family of oxides the MI transition seems to occur without any noticeable changes in lattice symmetry, which makes easier the study of the different phenomena involved. The transition temperature T_{MI} rises systematically as the rare-earth size becomes smaller, i.e., as the distortion of the perovskite with respect to the ideal structure (aristotype) increases (2). For $LaNiO_3$ the large size of La determines a slightly distorted rombohedral structure (space group $R\bar{3}c$) which, in fact, keeps its metallic character down to 1.5 K, showing no MI transition (3). $RNiO_3$ oxides (R = Pr, Nd, Sm, Eu) are orthorhombic, crystallize in the $GdFeO_3$ structure (space group *Pbnm*), and exhibit MI transitions at 130 (Pr), 200 (Nd), 400 (Sm), and 460 K (Eu) (2).

Reliable structural information about some of these perovskites has been obtained by neutron powder diffraction for R = La, Pr, Nd (4). The precise knowledge of the crystal structure of these phases has shown to be of paramount importance in the interpretation of the MI transitions, the temperature of which can be correlated to the Ni–O–Ni angles, governing the transfer integral between Ni-3*d* and O-2*p* orbitals. For R = Sm or Eu, the high neutron absorption cross section did not allow us to perform such structural studies for the corresponding perovskites. The structure of $SmNiO_3$ was refined from X-ray diffraction data (1) but, hitherto, no structural information about $EuNiO_3$ is available; this is probably due to the difficulties inherent to the stabilization of this perovskite, of metastable character, which must be prepared under high oxygen pressure. Only the unit-cell parameters of $EuNiO_3$ have been previously reported by Démazeau *et al.* (5), $a = 5.293$, $b = 5.466$, $c = 7.542$ Å, who prepared the complete series of $RNiO_3$ perovskites (R = Y, La, Nd, Sm, Eu, Gd, Dy, Ho, Er, Tm, Yb, Lu) under 60 kbar of oxygen pressure.

In the course of our current research about rare-earth nickelates, we were able to prepare a sufficiently pure $EuNiO_3$ powder sample, working at a moderate oxygen pressure of 200 bar. The aim of this paper is to report the preparation and structural data of $EuNiO_3$, to discuss some structural features on the light of a bond-valence study, and to characterize the MI transition of this perovskite by differential scanning calorimetry above room temperature.

EXPERIMENTAL

$EuNiO_3$ was prepared as a black polycrystalline powder starting from stoichiometric amounts of analytical grade Eu_2O_3 and $Ni(NO_3)_2 \cdot 6H_2O$, which were solved in citric acid. The citrate solution was slowly evaporated and decomposed at temperatures up to 600°C. All the organic materials were eliminated in a subsequent treatment at 800°C in air, after which the sample was slowly heated (1°C min^{-1}) up to 1000°C under 200 bar of oxygen pressure and held at this temperature for 12 hr. The product was finally cooled at 300°C hr^{-1} to room temperature.

X-ray powder diffraction (XRD) patterns were collected

[1] To whom correspondence should be addressed.

0022-4596/95 $12.00

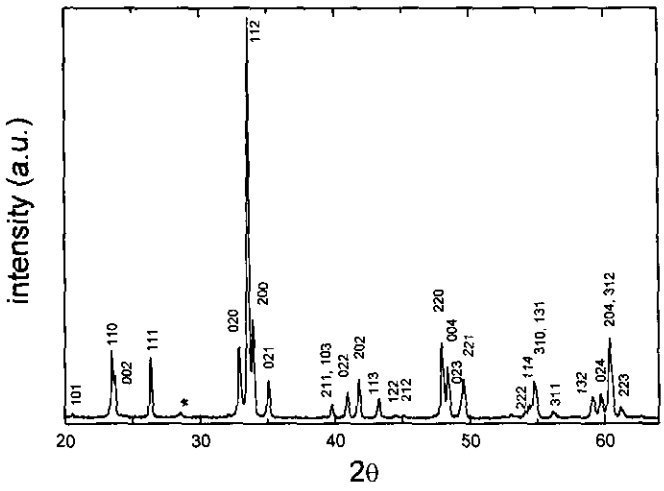

FIG. 1. XRD pattern of $EuNiO_3$, indexed on the basis of the orthorhombic $GdFeO_3$-type perovskite structure. The star indicates the most intense reflection of Eu_2O_3.

with Cu$K\alpha$ radiation in a Siemens D-501 goniometer controlled by a DACO-MP computer. For the structural refinement the diagram was recorded by step-scanning from 10° to 130° in 2θ, in increments of 0.025° and a counting time of 15 sec each step. The XRD pattern was analyzed by the Rietveld (6) method, using a strongly modified version (7) of the Wiles and Young refinement program (8). A pseudo-Voigt function was chosen to generate the line shape of the diffraction peaks. No regions were excluded in the refinement. Since small amounts of unreacted NiO (with rock-salt structure) and Eu_2O_3 were detected in the pattern, the profile refinement of the mixture was performed. In the final run the following parameters were refined: background coefficients, zero-point, half-width, pseudo-Voigt, and asymmetry parameters for the peak shape; scale factors, positional, and unit-cell parameters. Isotropic thermal factors were set to 0.3 and 0.7 Å^2 for metals and oxygen atoms, respectively, and an overall thermal factor was also refined.

Differential scanning calorimetry (DSC) experiments were performed in a Mettler TA3000 system equipped with a DSC30 unit, the temperature range 300 to 863 K. The heating rate was 10°C min^{-1}, using about 70 mg of sample in each run.

RESULTS AND DISCUSSION

$EuNiO_3$ was obtained as a black, well crystallized powder. The XRD diagram is characteristic of a perovskite showing sharp, well defined superstructure reflections corresponding to an orthorhombic distortion of the aristotype (ideal cubic perovskite, $a_0 \approx 4$ Å) with unit-cell parameters related to a_0 as $a = \sqrt{2}a_0$, $b = \sqrt{2}a_0$, $c = 2a_0$. Figure 1 shows the indexed XRD diagram, and Table 1 includes the observed and calculated d-spacings and observed intensities. The structural refinement was performed by the Rietveld method taking as starting parameters those of the $SmNiO_3$ structure (1). The final atomic coordinates, unit-cell parameters, and discrepancy factors after the refinement are included in Table 2. Figure 2 shows the goodness of the fit. The amount of Eu_2O_3 and NiO detected in the

TABLE 1
Miller Indices, Observed and Calculated d-Spacings, and Observed Intensities of the Peaks of the XRD Pattern of $EuNiO_3$

hkl	d_{obs}	d_{cal}	I/I_1
101	4.32(1)	4.32	3
110	3.79(1)	3.79	19
002	3.76(1)	3.76	12
111	3.39(1)	3.39	18
020	2.722(5)	2.723	20
112	2.668(4)	2.671	100
200	2.641(4)	2.643	27
021	2.561(4)	2.561	11
211	2.266(3)	2.268	5
103			
022	2.204(3)	2.207	7
202	2.162(2)	2.163	11
113	2.093(2)	2.093	7
122	2.033(2)	2.037	2
212	2.008(2)	2.011	2
220	1.897(2)	1.898	21
004	1.882(2)	1.882	16
023	1.845(2)	1.846	8
221	1.841(2)	1.840	12
123	1.746(2)	1.743	2
222	1.697(2)	1.696	4
114	1.687(1)	1.686	5
310	1.675(1)	1.675	11
131			
311	1.639(1)	1.637	3
132	1.563(1)	1.563	8
024	1.549(1)	1.549	7
204	1.533(1)	1.532	21
312			
223	1.514(1)	1.514	4

TABLE 2
Room Temperature Structural Parameters for $EuNiO_3$

Atom	Site	x/a	y/b	z/c	B (Å^2)
Eu	4c	0.9861(2)	0.0569(1)	0.25	0.3
Ni	4b	0.5	0	0	0.3
O1	4c	0.0913(18)	0.4828(15)	0.25	0.7
O2	8d	0.7101(16)	0.2901(15)	0.0422(10)	0.7

Note. $a = 5.2938(1)$, $b = 5.4560(1)$, $c = 7.5359(2)$ Å; space group $Pbnm$, $Z = 4$. $B_{ov} = -0.17$ Å^2. $R_p = 5.63$, $R_{wp} = 7.20$, $R_{exp} = 5.51$, $R_I = 3.24\%$; $\chi^2 = 1.71$.

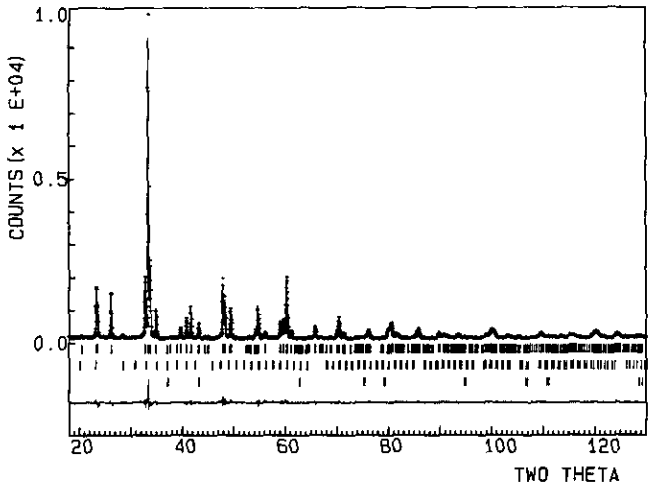

FIG. 2. Observed (crosses), calculated (solid line), and difference (at the bottom) XRD profiles for $EuNiO_3$ at 295 K. The three series of tick marks indicate the positions of the allowed Bragg reflections for the main phase, Eu_2O_3, and NiO. For the sake of clarity, only half of the experimental points are represented.

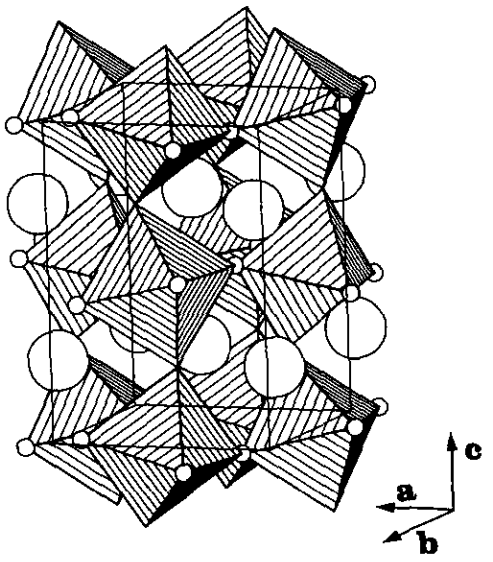

FIG. 3. View of the $EuNiO_3$ structure. O1 are in the apical positions of the NiO_6 octahedra. Small and large circles represent O2 and Eu, respectively.

diagram could be estimated from the scale factors to be lower than 0.5% in volume.

Table 3 contains a selected list of distances and angles, and a view of the structure is shown in Fig. 3. The perovskite structure of $EuNiO_3$ is fairly distorted due to the small size of the Eu^{3+} cations, which force the NiO_6 octahedra to tilt in order to optimize the Eu–O distances. The tilting description proposed by O'Keefe and Hyde (9) for the orthorhombic $GdFeO_3$-type perovskites (standard space group *Pnma*) involves main rotation axes in the $(0\,\bar{1}\,1)$ planes of the arystotype[2]. In the space group *Pbnm*, the rotation angle φ can be obtained from the z parameter of the oxygen at 8(*d*), as $\varphi = \text{arctg}[z(O2)\sqrt{48}]$. The refinement of the XRD data of $EuNiO_3$ led to $z(O2) = 0.042$, therefore, $\varphi = 16.2°$. For the sake of comparison, the same calculation has been performed for the other members of the $RNiO_3$ series (R = La, Pr, Nd, Sm, Ho) for which structural data are available (Table 4). A progressive increase of the tilting angle is observed as the rare-earth size decreases, except for Eu and Sm which display an almost similar φ value. Rotation angles within a similar range of

TABLE 3
Selected Distances (Å) and Angles (°) for $EuNiO_3$

Ni–O1	(×2)	1.947(2)	Eu–O1		2.273(10)
Ni–O2	(×2)	1.941(8)	Eu–O1		2.390(8)
Ni–O2	(×2)	1.960(8)	Eu–O1[a]		3.083(10)
⟨Ni–O⟩		1.949(6)	Eu–O1[a]		3.181(8)
			Eu–O2	(×2)	2.377(8)
			Eu–O2	(×2)	2.491(8)
			Eu–O2	(×2)	2.637(8)
			Eu–O2[a]	(×2)	3.319(8)
			$\langle Eu–O\rangle_{8\ short}$		2.459(8)
			⟨Eu–O⟩		2.715(8)
O1–Ni–O2		91.3(5)	Ni–O1–Ni		150.7(4)
O1–Ni–O2		90.5(5)	Ni–O2–Ni		153.9(15)
O2–Ni–O2		90.1(6)			

[a] Long Eu–O distances.

[2] For undistorted octahedra, a main rotation of φ demands a secondary tilt (of the octahedra and the primary axes) of $\pm\psi$ about an axis normal to the first, as $\psi = \tan^{-1}[\sqrt{2}(1 - \cos\varphi)/(2 + \cos\varphi)]$ (Ref. 9).

TABLE 4
Tilting Angle of the NiO_6 Octahedra, Mean Ni–O and R–O Distances, Tolerance t Factors, and Lattice Volumes for the $RNiO_3$ Perovskites

R	Ref.	φ^a	⟨Ni–O⟩	⟨R–O⟩	t	V (Å^3)
La	(4)	9.0	1.934(1)	2.632(1)	0.962	339.06(2)[b]
Pr	(4)	13.4	1.942(1)	2.541(3)	0.925	222.36(1)
Nd	(4)	14.7	1.942(3)	2.514(6)	0.915	220.71(1)
Sm	(1)	16.4	1.955(6)	2.468(8)	0.893	219.25(2)
Eu	This work	16.2	1.949(6)	2.459(8)	0.892	217.66(1)
Ho	(5)	18.0	1.938(5)	2.419(9)	0.883	211.96(25)

[a] For rhombohedral $LaNiO_3$ ($R\bar{3}c$) the tilting angle φ is obtained from the x coordinate of the oxygen position at (x 0 1/4), as $\varphi = \text{arctg}[x(O)\sqrt{12} - \sqrt{3}]$. For orthorhombic (*Pbnm*) $RNiO_3$ (R = Pr, ..., Ho), φ is calculated from the z coordinate of O2, at (x y z), as $\varphi = \text{arctg}(z(O2)\sqrt{48})$ (Ref. 9).

[b] For rhombohedral $LaNiO_3$ ($R\bar{3}c$, Z = 6) the normalized volume corresponding to 4 formula units (to compare with the orthorhombic structures, *Pbnm*, Z = 4) is 226.04(2) Å^3.

values have been reported for other perovskite series, such as the lanthanoid orthoferrites $RFeO_3$, in which a sequence across a range of φ from 15° to 23° has been observed (10).

The relative distortion of $EuNiO_3$ with respect to the other members of the $RNiO_3$ perovskites can also be discussed in terms of the tolerance factor, defined as $t = d_{R-O}/\sqrt{2}d_{Ni-O}$ (11), in the framework of a purely ionic model. Below $t = 1$ (corresponding to the cubic aristotype), the smaller the value of t, the larger the degree of distortion of the structure. Table 4 also includes the average ⟨Ni–O⟩ and ⟨R–O⟩ distances obtained from neutron (4) or X-ray (1, 5) diffraction data, the tolerance factors, and the unit-cell volumes of the $RNiO_3$ perovskites. It should be noticed that the tolerance factors for $EuNiO_3$ and $SmNiO_3$ are very close, which again suggests a similar magnitude of the distortion for both perovskites and is consistent with the close values of the φ tilting angle of the NiO_6 octahedra determined in both compounds from the z(O2) atomic parameters.

The fact that the ⟨Ni–O⟩ distances progressively increase from the La to the Sm perovskites in spite of the decrease observed in the lattice volume as R becomes smaller is striking. This behavior can be correlated with the chemical nature of the rare-earth cations present in the $RNiO_3$ phases. The large, basic La^{3+} cations are suitable to stabilize the highly charged Ni^{3+} cations: along the La–O–Ni bonds, La^{3+} allows the electronic density to be preferably shifted toward the short Ni–O bonds. With smaller, more acid R^{3+} cations as a partner, some electron density is progressively kept in the somewhat more covalent R–O bondings, thus weakening (lengthening) the Ni–O bonds. This effect is predominant for R ranging from La to Sm; for smaller rare earths the reduction in volume, which scales with the reduction in R^{3+} size and plays in the opposite direction, becomes predominant and explains the progressive decrease of ⟨Ni–O⟩ distances from Sm to Ho.

The trend to optimize the Eu–O bond lengths through the tilting of the octahedra can be easily checked by the calculation of the valence of the cations and anions present in the solid, following the Brown's bond valence model (12, 13). This model gives a phenomenological relationship between the formal valence of a bond and the corresponding bond length. In perfect nonstrained structures the bond valence sum (BVS) rule states that the formal charge of the cation (anion) is equal to the sum of the bond valences around this cation (anion). This rule is satisfied only if the stress introduced by the coexistence of different structural units can be relieved by the existence of enough degrees of freedom in the crystallographic structure. The departure of the BVS rule is a measure of the existing stress in the bonds of the structure.

Table 5 lists the valences calculated for Ni, Eu, and O from the individual Ni–O and Eu–O distances of Table 3. Ni and Eu atoms exhibit valences of 2.90 and 3.18 v.u., respectively, somewhat below or above the expected value of +3 for both cations. This fact seems to indicate that Ni cations are slightly underbonded and hence Ni–O bonds are under tensile stress, whereas Eu cations are overbonded and under compressive stress, giving rise to a structure with some metastable character (this is useful to compare with the $LaNiO_3$ structure (4), in which Ni and La exhibit valences of +3.01 and 3.00 v.u., respectively).

TABLE 5

Bond Valences[a] (s_i) for Eu–O and Ni–O Bonds, Multiplicity of the Bonds [m], and Valences (Σ_{s_i}) for Eu, Ni, and O Atoms within the Respective Coordination Polyhedra in the $EuNiO_3$ Structure

Atom	s_i, [m]				Σ_{s_i}
Eu	0.59, [1]	0.43, [1]	0.07, [1]	0.05, [1]	
	0.44, [2]	0.33, [2]	0.22, [2]	0.03, [2]	3.18
Ni	0.49, [2]	0.49, [2]	0.47, [2]		2.90
O1	0.59, [1]	0.43, [1]	0.49, [2]	0.07, [1]	
	0.05, [1]				2.12
O2	0.44, [1]	0.33, [1]	0.22, [1]	0.49, [1]	
	0.47, [1]	0.03, [1]			1.98

[a] Bond valences are calculated as $s_i = \exp[(r_0 - r_i)/B]$; $B = 0.37$; r_0(Eu) = 2.076, r_0(Ni) = 1.68 Å for the Eu^{III}–O^{2-} and Ni^{II}–O^{2-} pairs, respectively (from Ref. 14)). Individual Eu–O and Ni–O distances are taken from Table 3.

The contrast between the almost regular NiO_6 octahedra observed in $RNiO_3$ for the largest rare earths (R = La, Pr, Nd) (4) and the distortion observed in the NiO_6 octahedra of $EuNiO_3$, in which Ni-O distances range between 1.94 and 1.96 Å, is also noteworthy. This distortion is still more evident in $HoNiO_3$, with Ni–O bond lengths in the range 1.92–1.96 Å (5). The origin of such behavior can be found in the "distortion theorem" enunciated by Brown and Shannon (12, 14), which states that "in any coordination sphere in which the average bond length is kept constant, any deviation of the individual bond lengths from this value will increase the valence sum at the central atom." If we consider Ni as the central atom of a coordination sphere formed by O anions, it follows from the theorem that the observed departure of the individual bond lengths with respect to the average value, thus increasing the distortion of the NiO_6 octahedra, is driven by the trend of the underbonded Ni cations to increase its valence.

Figure 4 shows the DSC curves for $EuNiO_3$ obtained during the heating and cooling runs, respectively. The heating process exhibits an endothermic peak centered at 189.3°C (462.5 K) corresponding to the first-order insulator-to-metal transition. The reverse transition is observed during the cooling run, showing an exothermic peak at 185.4°C (458.6 K). The observed thermal hysteresis is inherent to the first-order character of the transition. The temperature transition is in good agreement with that de-

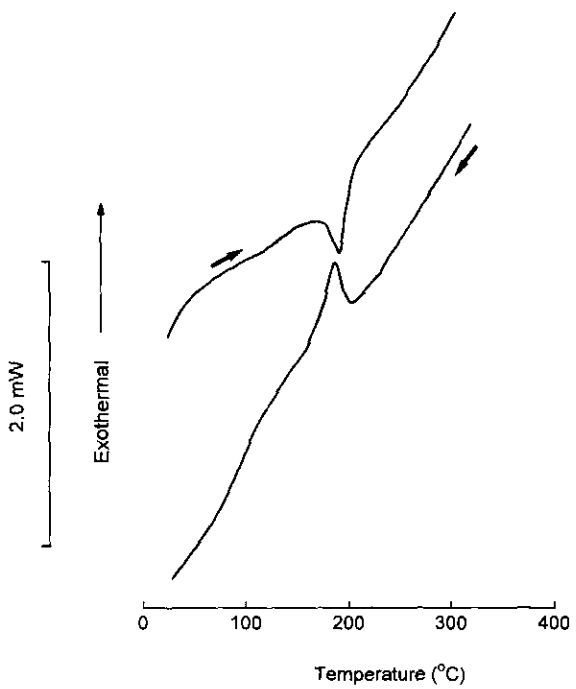

FIG. 4. DSC curves, obtained on heating and cooling, of $EuNiO_3$.

termined elsewhere (2) from the endothermic DSC peak and resistivity measurements (460 K).

The values obtained for the enthalpy changes are $\Delta H = 184$ J mole^{-1} and $\Delta H = 190$ J mole^{-1} for the endothermic and the exothermic processes, respectively. These figures are much lower than those reported for the insulator-to-metal transition of $NdNiO_3$, 353 J mole^{-1} (15) or 376 J mole^{-1} (16) during the heating process. The origin of such a difference can be found in the fact that $NdNiO_3$ undergoes an antiferromagnetic-to-paramagnetic transition associated, at the same temperature (203 K on heating (15)), to the insulator-to-metal transition, whereas in the highly distorted compounds such as $SmNiO_3$ or $EuNiO_3$ there is a clear separation between both transitions. The Néel temperature of $EuNiO_3$, determined from positive muon-spin relaxation (μ^+SR), is 205 K, dramatically lower than that found for the insulator-to-metal transition (2). Hence, the heat transfer observed at 463 K accounts only for the gain in energy corresponding to the electronic delocalization when reaching the metallic state, above this temperature.

CONCLUSIONS

A citrate route was shown to be an adequate synthesis procedure for the obtention of the highly metastable $EuNiO_3$ perovskite. This compound is the last member of the $RNiO_3$ series that can be prepared at moderate oxygen pressures ($P \leq 200$ bar). $EuNiO_3$ crystallizes in a very distorted orthorhombic perovskite structure, with a tolerance factor $t = 0.892$. The observed valences for Ni and Eu, determined from bond valence considerations, are slightly lower or higher, respectively, than the expected value of +3 for both cations. This fact could be in the origin of the metastable character of the structure. The MI transition of $EuNiO_3$ shows the hysteretic behavior expected for a first-order transition, as shown by DSC measurements. The heat transfer corresponding to the MI transition of $EuNiO_3$ (at ~460 K) is by far lower than that observed for $NdNiO_3$ (at ~200 K); in the latter compound the MI transition is associated to a paramagnetic-antiferromagnetic transition, whereas in the former perovskite the magnetic ordering takes place at much lower temperatures, of about 205 K.

ACKNOWLEDGMENT

The authors acknowledge the financial support of the DGICYT to Project PB91-0089.

REFERENCES

1. P. Lacorre, J. B. Torrance, J. Pannetier, A. I. Nazzal, P. W. Wang, and T. C. Huang, *J. Solid State Chem.* **91,** 225 (1991).
2. J. B. Torrance, P. Lacorre, A. I. Nazzal, E. J. Ansaldo, and Ch. Niedermayer, *Phys. Rev. B* **45,** 8209 (1992).
3. J. B. Goodenough and P. Raccah, *J. Appl. Phys.* **36,** 1031 (1965).
4. J. L. García-Muñoz, J. Rodríguez-Carvajal, P. Lacorre, and J. B. Torrance, *Phys. Rev. B* **46,** 4414 (1992).
5. G. Démazeau, A. Marbeuf, M. Pouchard, and P. Hagenmuller, *J. Solid State Chem.* **3,** 582 (1971).
6. H. M. Rietveld, *J. Appl. Crystallogr.* **2,** 65 (1969).
7. J. Rodríguez-Carvajal, "FULLPROF: A Program for Rietveld Refinement and Pattern Matching Analysis; Abstracts of the Satellite Meeting of the XVth Congress of the International Union of Crystallography," p. 127. Toulouse, 1990.
8. D. B. Wiles and R. A. Young, *J. Appl. Crystallogr.* **14,** 149 (1981).
9. M. O'Keefe and B. Hyde, *Acta Crystallogr. Sect B* **33,** 3802 (1977).
10. M. Marezio, J. P. Remeika, and P. D. Dernier, *Acta Crystallogr. Sect B* **26,** 2008 (1970).
11. J. B. Goodenough and J. M. Longo, *in* "Magnetic and Other Properties in Oxides and Related Compounds" (K. H. Hellwege and A. M. Hellwege, Eds.), Landolt-Börnstein, New Series, Group III, Vol. 4a, Chap. 3, p. 126. Springer-Verlag, Berlin, 1970.
12. I. D. Brown, *in* "Structure and Bonding in Crystals" (M. O'Keefe and A. Navrotsky, Eds.), Vol. 2, p. 1. Academic Press, New York, 1981.
13. N. E. Brese and M. O'Keefe, *Acta Crystallogr. Sect. B* **47,** 192 (1991).
14. I. D. Brown and R. D. Shannon, *Acta Crystallogr. Sect. A* **29,** 266 (1973).
15. X. Granados, J. Fontcuberta, X. Obradors, Ll. Mañosa, and J. B. Torrance, *Phys. Rev. B* **48,** 11666 (1993).
16. J. A. Alonso, M. J. Martínez-Lope, and M. A. Hidalgo, *J. Solid State Chem.* **116,** 146 (1995).